Accounting for Rough Bed Friction Factors of Mud Beds as a Result of Biological Activity in Erosion Experiments

Katell Guizien, Francis Orvain, Jean-Claude Duchêne, Pierre Le Hir

Accounting for rough bed friction factors of mud beds due to biological activity in erosion experiments

Katell Guizien[1], Francis Orvain[2], Jean-Claude Duchêne[3], Pierre Le Hir[4]

April 12, 2012

[1] CNRS/Université Paris 06, FRE3350, LECOB, Observatoire Océanologique, rue du Fontaulé, F-66650, Banyuls/mer, France

[2] Laboratoire PE2M (Physiologie et Ecophysiologie des Mollusques Marins), Université de Caen, Esplanade de la Paix, F-14032 Caen CEDEX, France.

[3] Université de Bordeaux, CNRS, UMR 5805-EPOC, Talence, F-33405 France

[4] IFREMER, Centre de Brest, BP70, F-29280 Plouzané, France.

Abstract

The average bed shear stress and bed friction factor of samples with any roughness was derived from the head loss between upstream and downstream of a test section in an erosion tunnel. The method was validated in both hydraulically smooth (plexiglass, Reynolds number less than 25,000) and rough regimes (calibrated particles with known roughness). As a first step toward using this method on natural sediment, we tested this method with experimental mesocosms assembled from field collected materials (sieved sediments, diatoms). Bed shear stress measurement precision was high enough in the experiments to detect a positive significant relationship between bed friction factor and core roughness. The observed bed friction factor increase could be related to diatom growth but not to diatoms biomass.

Introduction

Erosion of fine grained sediment and any living or dead benthic biota associated with sediment particles are key processes in the control of coastal ecosystems' primary and secondary productivities and their morphodynamics which remain difficult to predict for field situations. Sediment erosion flux results from the balance between bed shear stress induced by fluid forcing and sediment erodibility (that is the sediment resistance to erosion). Muddy sediment erodibility were first studied by focusing on abiotic factors (grain size, mineralogy, salt and water content, Mehta et al. 1982; Parchure and Mehta 1985; Mehta 1986). Devices for field studies of erosion opened the way in the 1990s for new investigations of biological parameters (biofilm, bioturbation) and sediment erodibility (e.g. Paterson 1989; Gust and Morris 1989; Amos et al. 1992; Widdows et al. 2000; Andersen et al. 2001; Black et al. 2002). Mud erodibility properties are expected to be best preserved with *in situ* flumes, although careful sampling technique and rapid transfer to the laboratory limit discrepancies between field and laboratory assessments (Tolhurst et al. 2000a,b; Widdows et al. 2007). Other concerns remained about the ability of either field or laboratory flumes to relate erodibility to fluid action (see review in Black & Paterson 1997, updated in Tolhurst et al. 2009). One criticism, which is cited repeatedly, is that flows are frequently non uniform in inverted benthic flumes, either across the flume section due to secondary flows in a horizontal annular recirculating flume, or along the flume axis in straight flow-through flumes of finite length due to a partially developed boundary layer (Aberle et al. 2003). Another, more important, concern is that bed shear stresses are (in most cases) not measured during erosion experiments (Gust and Morris 1989), but derived from flow velocity using pre-deployment calibrations (Amos et al. 1997; Widdows et al. 1998; Andersen et al. 2001; Aberle et al. 2003; Orvain et al. 2007). Bed shear stress, however, depends not only on flow velocity, but also on the bottom roughness. Thus, a predeployment calibration implicitly assumes that field mud bed roughness is the same as the one used for calibration (generally hydraulically smooth, except in Andersen et al., 2001 and Aberle et al., 2003). Under low bed shear stresses ($<\sim 0.5$ Pa), it is possible that the shear flow in small erosion devices remains hydraulically smooth, even in the presence of naturally rough beds (Cartwright et al. 2009). Nonetheless,

the hydraulically smooth assumption might not be valid in natural settings (Debnath et al. 2007) and at high Reynolds number during the erosion experiment. Hence, if one aims to investigate the relation between erodibility and ecological factors or extrapolate erodibility measurements in erosion modelling, we must be able to relate erodibility to the actual bed shear stress applied and accounting for the effective mud roughness.

This study uses head loss between the upstream and downstream of a test section in a laboratory recirculating tunnel to derive the actual averaged bed shear stress over samples with any roughness. The sensitivity to bed roughness of the method was checked with smooth (plexiglass) and rough (made of calibrated particles) beds. Finally, we investigated the relationship between bed friction factors derived from bed shear stress measurements over muddy sediment having growing diatoms and/or bioturbating fauna, and the roughness estimate derived from core surface topography.

Material and Methods

The Erodimetre erosion tunnel and principles for measurement of averaged bed shear stress over core samples

The Erodimetre erosion tunnel of the *Institut Français de Recherche pour l'Exploitation de la MER* (IFREMER) is a small recirculating straight tunnel made of plexiglass (1.20 m long, a=8 cm wide and b=2 cm high, Fig. 1) designed to perform *ex situ* experiments (Le Hir et al. 2007). The hydraulic diameter of the duct's rectangular section is $D_h = 2ab/(a+b) = 3.2$ cm. Erosion experiments can be done on duplicate sediment cores (8 cm diameter) placed flush with the bottom in a 36 cm long section at the downstream end of the tunnel (Fig. 1). The test section is located 80 cm downstream from the tunnel entrance to ensure a fully developed and steady boundary layer at the entrance of the test section for flow discharge up to 1.75 l s^{-1}(Schlichting 1979). Sand paper with a roughness height of 115 μm was glued on the tunnel bottom upstream of the test section to diminish roughness changes at the tunnel bottom to test section transition for hydraulically rough samples. A large artificial roughness was added to the top of the tunnel to homogenize

the bed shear stress across the tunnel (Le Hir et al. 2006; Calluaud and Mouazé 2007). The flow discharge delivered by the recirculating pump is continously gauged by a flow meter. Discharge may be varied from 0 and 2.5 l s^{-1} by steps of 0.1 l s^{-1}, corresponding to a discharge velocity U ranging from 0 to 1.56 m s^{-1}, by steps of 0.0625 m s^{-1} (Reynolds number $Re = UD_h/\nu$ up to 50,000 using the kinematic viscosity $\nu = 10^{-6}$ m^2 s^{-1} for water). A differential pressure gauge measures the total pressure difference Δp between two sections 36 cm apart, (that is, upstream and downstream of the test section), with a resolution of 1 Pa. A negative total pressure difference indicates head loss $\Delta h = \Delta p/(\rho g)$ in the test section, with ρ, the fluid density and g, the Earth's gravity acceleration. Head loss between tunnel cross sections located upstream and downstream of the test section (Figure 2a) may be used to directly determine the average bed shear stress over the core samples (Briaud et al. 2001).

Substracting equations of steady state momentum balance between upstream and downstream the test section with plexiglass caps and samples with any roughness, the average bed shear stress on rough samples τ_{rough} yields:

$$\tau_{\text{rough}} = \tau_{\text{smooth}} + \frac{S_1}{2S_3}[\Delta h_{caps} - \Delta h_{core}] \tag{1}$$

where τ_{smooth} and Δh_{caps} are the average bed shear stress and head loss, respectively, over hydraulically smooth plexiglass caps replacing cores in the test section, S_1 is the tunnel cross-section area, S_3 is the core area and, Δh_{rough} is the head loss with rough cores. The last term in equation (1) is the excess bed shear stress due to the core roughness compared to hydraulically smooth plexiglass caps (Fig. 2).

Bed shear stress τ can be related to discharge velocity introducing a bed friction factor f defined as:

$$\tau = \rho f U^2/8 \tag{2}$$

In pipes, τ_{smooth} can be calculated using the Reynolds dependent friction factor value given in the Moody chart for smooth walls (Moody 1944). In the Erodimetre, τ_{smooth} should be lower than the bed shear stress measured with plexiglass caps τ_{caps}:

$$\tau_{caps} = \rho g \frac{S_1}{2(\Sigma + S_2)} \Delta h_{caps} \tag{3}$$

where S_2 is the area of the smooth side-wall of the test section and Σ is the area of the top-wall of the test section where roughness were added. At least, one "cap" experiment was performed during each experimental series; a sixth degree polynomial was fitted to describe the Δh_{caps} as a function of the flow discharge.

It should be noted that at zero discharge, the pressure gauge resolution of 1 Pa limits the precision of bed shear stress determinations to 0.16 Pa. Moreover, discharge fluctuations induce head fluctuations that may reach 0.1 cm at high flow discharges (Fig. 2b), leading to practical uncertainties on the bed shear stress determination that were estimated at $\pm$ 0.5 Pa for discharge ranging from 0.1 l s^{-1} to 2.5 l s^{-1}.

Shields experiments

Experiments with calibrated particles were carried out in tap water to test the accuracy of the bed shear stress determination based on head loss. The core surface was uniformly covered by a 1 cm thick layer of calibrated particles, ensuring a plane surface flush with the tunnel bed and the discharge was increased. According to Shields (1936) diagram, particles with median diameter D_{50} start to move when the bed shear stress reach a critical value, $\tau_{Shields}(D_{50})$, defined as (Soulsby 1997):

$$\frac{\tau_{Shields}(D_{50})}{g(\rho_s - \rho)D_{50}} = 0.055\,[1 - \exp(-0.02D^*)] + \frac{0.3}{1 + 1.2D^*} \tag{4}$$

where ρ_s is particles density and D^* is the dimensionless particle diameter, defined as $D^* = [g(\rho_s/\rho - 1)/\nu^2]^{1/3} D_{50}$.

Characteristics of the calibrated particles, including the relative roughness height value (D_{50}/D_h), used in these Shields experiments are given in Table 1. Critical bed shear stress and the corresponding particle Reynolds number $RE_c = UD_{50}/\nu$ value are also reported. These critical bed shear stress values were compared to the bed shear stress values derived from the measured head loss when particles started to move. For each experiment with calibrated particles, a mean value and standard deviation of bed friction factor f was calculated by a linear regression between bed shear stress and the square of flow velocity for discharges larger than 0.15 L s^{-1}.

Mesocosm experiments

Experiments were carried out in sea water using reconstructed cores from natural sediment (10 μm median grain size) collected on the intertidal mudflats of Marennes-Oléron Bay (French Atlantic coast). Sediment collected were sieved to 1 mm to remove any macrofauna.

The experiments were designed to explore the relationship between the development stage of a microphytobenthic biofilm and mud surface roughness. To simulate different diatom biofilm development stages, twenty reconstructed mud cores were inoculated with benthic diatoms, twenty were not and all were pre-conditioned in the same tidal mesocosm for 5 days before an erosion experiment. Twenty cores without added diatoms were pre-conditioned at the same time. Two erosion experiments were then carried out every two days over a period of eight days, one with cores that had microphytobenthos added, and the second without. Two mud cores were placed in the Erodimetre and flow increased until mass erosion occurred (detachment of centimetric sediment aggregates, detected visually). The diatom biomass was estimated by analyzing the pigments present in the uppermost centimeter of mesocosm cores (Lorenzen 1967).

Before and after each of the experiments, a high resolution scan of cores' surface topography was done over a 5 cm $\times$ 5 cm area at the core center at a horizontal resolution of 200 μm $\times$ 200 μm. The surface topography is the vertical deviation of the core surface from an average horizontal plane measured at a 15 μm vertical resolution and core roughness was the square root of the variance of the core topography.

Finally, a bed shear stress-pump discharge curve was established for each experiment. One experiment was excluded as the cores surface was perfectly flush with the tunnel bed, presenting upward and downward steps to the flow (Briaud et al. 2001) which produced unexpected large bed shear stresses. These outlying values highlight the difficulty in placing natural samples flush with the tunnel bed. Mean values and standard deviations for the bed friction factor were calculated after a linear regression between bed shear stress and the square of discharge velocity for discharges from 0.35 to 1.75 L s^{-1} (Re from 7,000 to 35,000). The linear relationship between bed friction factor and core roughness was also tested.

Results and Discussion

This paper uses head loss measurement to derive bed shear stress as a function of discharge in both hydraulically smooth and rough regimes (Fig. 3). Briaud et al. (2001) also attempted to use head loss measurements to derive bed shear stress, although no details were given on how the authors dealt with the differential roughness between the tunnel walls and the sample when deriving bed shear stress from head loss measurements. After comparing erosion flux measurements in tunnel and flume experiments, they argued that using the Moody chart (Moody 1944) was more appropriate to relate erosion flux to bed shear stress in the tunnel. However, using the Moody chart in a hydraulically rough regime requires knowing the sample roughness which is generally not the case in natural settings, particularly when roughness arises from biological activity and along an erosion experiment. The method presented in this study derives bed shear stress along erosion experiments over samples with unknown roughness. The method performance was checked over a wide range of sample roughness (plexiglass, calibrated particles, mud with biological activity). Bed shear stress derivation from head loss measurement when the test section was made of plexiglass deviated by less than a few percent from bed shear stress calculated with equation (2) using the hydraulically smooth Moody chart friction factor if the Reynolds number was less than 25,000 (Fig. 3a). Smooth bed shear stress values ranged from 0 to 6 Pa at 2.5 L s^{-1} but remained below 1 Pa for discharges lower than 1 L s^{-1}. For Reynolds numbers greater than 25,000, bed shear stress values were larger than Moody chart smooth regime predictions and varied by 30 % between different repeated experiments. Deviation may be due to the development of a rough boundary layer on the top wall and the adaptation of the rough bed boundary layer that had established over rough sand paper between the tunnel entrance and the test section to the abrupt roughness change over smooth plexiglass caps. Thus, Moody chart prediction was used for the smooth bed shear stress value in equation (1).

When the plexiglass caps were replaced by surfaces made of calibrated particles, bed shear stress values increased by around a factor 10, reaching the hydraulically rough regime (Fig. 3a, $RE_c > 70$). Average bed friction factors derived using equation (2) were close for beds made of either sand or steel particles but having the

same median diameter and increased significantly when median diameter increased (Table 1). The hydraulic roughness of plane beds formed by particles with uniform size (Nikuradse 1933) was derived from these bed friction factor after integration of the velocity logarithmic profile over its thickness (6 mm according to, Calluaud and Mouazé 2007)). Hydraulic roughnesses ranged from 2.1 to 2.6 times the mean diameter of bed particles, which is within values generally observed over a plane bed made of sand grains (Guy et al. 1966). Finally, the values of measured bed shear stress when calibrated particles start to move agreed fairly well with bed shear stress values predicted by Shields criteria (equation 4, deviation lower than 20 % at high flow, Fig. 4), demonstrating the accuracy of bed shear stress determinations based on head loss measurements. This validation accounted for uncertainties of about 1 Pa due to the observer difficulty in appreciating when particles start to move. A similar method was used to convert into equivalent bed shear stress either the eroding pressure of the pulsating jet of a Cohesive Strength Meter (Tolhurst et al. 1999) or the propeller revolution velocity for the EROMES device (Andersen et al. 2001). In the present study, validation of the method covered a wide range of bed shear stress values (from 0.15 to 12.7 Pa) which may prove to be useful to study the erosion of consolidated muds. In any case, bed shear stress range was larger than the usual range (up to 3 Pa) of erosion devices calibrated with smooth walls (Amos et al. 1997; Widdows et al. 1998), and close to bed shear stress values obtained when calibrating the NIWA flume with an artificial rough surface (Aberle et al. 2003). In summary, the method based on head loss between upstream and downstream, a test section with reduced length (ten times the hydraulic diamater) in the Erodimeter performed better in the hydraulically rough regime (20 % precision on bed shear stress determination) than in the hydraulically smooth regime. This should be attributed to the effort in reducing roughness change at the transition between the sample and the tunnel bottom covered with sand paper of intermediate roughness. Precision could be increased using a longer test section to ensure a fully developed boundary layer in the test section.

Six bed shear stress-flow discharge curves were measured over mud cores, three of which were enriched with diatom (Fig. 3). Bed shear stresses over muddy sediment supporting diatom growth increased by up to a factor of 4 compared to the smooth bed shear stresses that may be expected for a 10 μm mud grain size. Meanwhile,

smooth bed shear stress predictions have been used extensively, in both field (Amos et al. 1997; Widdows et al. 1998; Orvain et al. 2007) and laboratory (Orvain et al. 2003; Ravens 2007) studies of natural mud beds' stability. Bed shear stress underestimation may have passed unnoticed when, for instance, lower critical bed shear stresses were found over bioturbated beds compared to non bioturbated beds and were interpreted as erodibility increase (Orvain et al. 2007). However, bed roughness enhancement after bioturbation would also lead to lower critical bed shear stress values if derived from calibration versus flow velocity over a smooth bed. In addition, flow velocity may indicate an erroneous hierarchy of sediment erodibility as bed roughness evolves during an erosion experiment (Maa et al. 1998).

The experimental series of the present study clearly showed a large variability (by a factor two) in bed shear stress values for the same discharge. Bed shear stress were lower when cores were not enriched with diatoms. Chlorophyll a concentration increased from 100 to 210 mg Chl a m^{-2} in the uppermost cm of sediment cores indicating diatom growth during the first 7 days of experiment. These values cover the range of chlorophyll a concentration observed over intertidal mudflats (Blanchard et al. 2001). Growth was slower in cores without diatom enrichment. Bed shear stress increased after 5 and 7 days of diatom growth and strongly decreased when diatom biomass stabilized 9 days after inoculation.

Bed friction factor f values ranged from 0.04 to 0.09, and were significantly correlated with core roughness ($R = 0.95$ and $p = 0.35\%$). Core surface topography was generally bumpy in its center mainly due to the way it was cored and slid into the tunnel bottom. Core roughness were larger on average with diatoms enrichment (3.1 mm) than without (1.8 mm). Rough bed friction factors found over mud cores in the present study indicated hydraulic relative roughness ranging from 0.012 to 0.05 using Moody chart predictions. Hydraulic roughnesses ranged from 2 to 4 times the roughness estimated from topography variance.

In any case, hydraulic roughness increase could be related to the microphytobenthic biofilm development but not to microalgal biomass integrated over the uppermost sediment centimeter. Biological enhancement of cohesive sediment hydraulic roughnesses have frequently been attributed to bioturbation by infauna or small epibenthic species (Nowell et al. 1981; Wright et al. 1997; Ciutat et al. 2007). To our knowledge, hydraulic bed roughness enhancement of mud interface

by biofilm coatings has never been shown, although previous studies have reported spatial micro-heterogeneity linked to discontinuous patches of diatoms at the sediment surface (Grant et al. 1986).

Conclusion

Head loss between the upstream and downstream of a test section in an erosion tunnel was used to derive the averaged bed shear stress and bed friction factor of samples with any roughness. The method was validated in both the hydraulically smooth regime (plexiglass, $Re < 25,000$) and rough regimes (calibrated particles with known roughness). The present study confirmed that *a priori* calibration of experimental devices relating bed shear stress to flow discharge assuming hydraulically smooth beds may be inadequate for studying erodibility of natural intertidal bare mudflats supporting diatom growth, especially at high stress conditions. However, reliable estimates of bed friction factor requires to repeat experiments when studying natural samples to detect any artefactual roughness due to sample not perfectly flush with the tunnel bed. Bed shear stress measurement precision was high enough to detect a relationship between bed friction factor and roughness produced by diatom biofilm growth. However, any roughness change should rather be related to biota activities than to biomass.

Acknowledgments

This work was supported by the French ANR (National Research Agency) through the VASIREMI project "Trophic significance of microbial biofilms in tidal flats" (contract ANR-06-BLAN-0393-01). The assistance of Caroline Nérot for the mesocosms experiments is gratefully acknowledged. We also thank Jennifer Coston-Guarini and Ian Salter for language correction.

Notation

The following symbols are used in this technical note:

$a =$ tunnel width (cm)

$b =$ tunnel height (cm)

$D_h =$ tunnel hydraulic diameter (cm)

$D_{50} =$ particles median diameter (mm)

$D^* =$ particles median diameter (dimensionless)

$f =$ bed friction factor (dimensionless)

$g =$ Earth gravity (m s^{-2})

$Re =$ tunnel Reynolds number (dimensionless)

$RE_c =$ particle Reynolds number (dimensionless)

$S_1 =$ tunnel cross section area (m^2)

$S_2 =$ test section side wall area (m^2)

$S_3 =$ core area (m^2)

$U =$ tunnel discharge velocity (m s^{-1})

$\Delta h =$ head loss between upstream and downstream of test section (m)

$\Delta h_{caps} =$ head loss between upstream and downstream of test section with plexiglass caps (m)

$\Delta h_{rough} =$ head loss between upstream and downstream of test section with rough sample (m)

$\Delta p =$ pressure difference between upstream and downstream of test section (Pa)

$\nu =$ fluid kinematic viscosity (m^2 s^{-1})

$\rho_s =$ particle density (kg m^{-3})

$\rho =$ fluid density (kg m^{-3})

$\Sigma =$ test section top wall area (m^2)

$\tau =$ bed shear stress (Pa)

$\tau_{caps} =$ average bed shear stress derived from equation (3) (Pa)

$\tau_{rough} =$ average bed shear stress over rough sample (Pa)

$\tau_{smooth} =$ bed shear stress over hydraulically smooth plexiglass caps (Pa)

$\tau_{Shields}(D_{50}) =$ bed shear stress value when particles with diameter D_{50} started to move (Pa)

References

Aberle, J., Nikora, V., McLean, S., Doscher, C., McEwan, I., Green, M., Goring, D., Walsh, J. (2003) "Straight Benthic Flow-Through Flume for In Situ Measurement of Cohesive Sediment Dynamics." *J. Hydraul. Eng.*, 129(1), 63-67

Amos, C.L., Grant, J., Draborn, G.R., Black, K. (1992) "Sea Carousel- a benthic,

annular flume." *Est. Coast. Shelf Sci.*, 34, 557-577.

Amos, C.L., Feeney, T., Stherland, T.F., Luternauer, J.L. (1997) "The stability of fine-grained sediments from Fraser river delta." *Est. Coast. Shelf Sci.*, 45, 507-524.

Andersen, T.J. (2001) "Seasonal variation in erodibility of two temperate microtidal mudflats." *Est. Coast. Shelf Sci.*, 53, 1-12.

Black, K.S., Paterson, D.M. (1997) "Measurement of the erosion potential of cohesive marine sediments: a review of current *in situ* technology." *J. Marine Env. Eng.*, 4, 43-83.

Black, K.S., Tolhurst, T.J., Paterson, D.M., Hagerthey, S.E. (2002) "Working with natural cohesive sediments." *J. Hydraul. Eng.*, 128(1), 1-7.

Blanchard, G.F., Guarini, J.-M., Orvain, F., Sauriau, P.G. (2001) "Dynamic behaviour of benthic microalgal biomass in intertidal mudflats." *J. Exp. Mar. Biol. and Ecol.*, 264, 85-100.

Bocher, P., Piersma, T., Dekinga, A., Kraan, C., Yates, M.G., Guyot, T., Folmer, E.O., Radenac, G. (2007) "Site- and species-specific distribution patterns of molluscs at five intertidal soft-sediment areas in northwest Europe during a single winter." *Mar. Biol.*, 151, 577-594

Briaud, J.L., Ting, F.C.K., Chen, H.C., Cao, Y., Kwak, K.W. (2001) "Erosion function apparatus for scour rate predictions." *J. Geotech. Geoenv. Eng.*, 127(2), 105-113.

Calluaud, D., Mouazé, D. (2007) "Soutien au calibrage de l'érodimètre de l'IFREMER." *IFREMER Tech. Report*, 38 p.

Cartwright, G.M., Friedrichs, C.T., Dickhudt, P.J., Gass, T., Farmer, F.H. (2009) "Using the acoustic Doppler velocimeter (ADV) in the MUDBED real-time observing system." Proceedings, *OCEANS 2009 MTS/IEEE*, CD ISBN: 978-0-933957-38-1, 9 p.

Ciutat, A., Widdows, J., Pope, N.D. (2007) "Effect of Cerastoderma edule density on near-bed hydrodynamics and stability of cohesive muddy sediments." *J. Exp. Mar. Biol. Ecol.*, 46(1-2), 114-126.

317 Debnath, K., Nikora, V., Aberle, J., Westrich, B., Muste, M. (2007) "Erosion of
318 Cohesive Sediments: Resuspension, Bed Load, and Erosion Patterns from Field
319 Experiments" *J. Hydraul. Eng.*, 133(5), 508-520

320 Grant, J., Bathmann, U.V., Mills, E.L. (1986) "The interaction between benthic
321 diatoms films and sediment transport." *Est. Coast. Shelf Sci.*, 23, 225-238.

322 Gust, G., Morris, M.J. (1989) "Erosion thresholds and entrainment rates of undis-
323 turbed *in situ* sediments." *J. Coast. Res.*, 5, 87-99.

324 Guy, H.P., Simons, D.B., Richardson, E.V. (1966) "Summary of alluvial channel
325 data from flume experiment, 1956-1961." US Geological survey, Prof paper 462-1,
326 Washington DC.

327 Le Hir, P., Cann, P., Jestin, H., Bassoulet, P. (2006) "Instrumentation légère pour
328 la mesure de l'érodabilité des sédiments vaseux ou sablo-vaseux." Proceedings
329 IXèmes Journées Nationales Génie Côtier-Génie Civil.

330 Le Hir, P., Monbet, Y., Orvain, F. (2007) "Sediment erodability in sediment trans-
331 port modelling: Can we account for biota effects ?" *Cont. Shelf Res.*, 27, 116-1142.

332 Lorenzen, C. (1967) "Determination of chlorophyll and phaeopigments spectropho-
333 tometric equations." *Limnol. Oceanogr.*, 12, 343 346.

334 Maa, J.P.-Y, Sandford, L., Halka, J.P. (1998) "Sediment resuspension characteristics
335 in Baltimore Harbor, Maryland." *Mar. Geol.*, 146, 137-145.

336 Mehta, A.J. (1986) "Characterisation of cohesive sediment properties and trans-
337 port processes in estuaries." In: Mehta, A.J. (Ed.), *Estuarine Cohesive Sediment*
338 *Dynamics*. Springer, Berlin, 290-325.

339 Mehta, A.J., Parchure, T.M., Dixit, J.G., Ariathurai, R. (1982) "Resuspension po-
340 tential of deposited cohesive sediment beds." In: Kennedy, V.S. Ed. *Estuarine*
341 *Comparisons.*, Academic Press, 591-609.

342 Moody, L.F. (1944) "Friction factors for pipe flow." Trans. Am. Soc. of Mech. En-
343 grs,66.

Nikuradse, J. (1933) "Stromungsgesetze in glatten und rauhen rohren." *VDI Forschungsheft*, 361, Berlin.

Nowell, A.R.M., Jumars, P.A., Eckman, J.E. (1981) "Effects of Biological Activity on the Entrainment of Marine Sediments." *Mar. Geol.*, 42(1-4), 133-153.

Orvain, F., Le Hir, P., Sauriau, P.-G. (2003) "A model of fluff layer erosion and subsequent bed erosion in presence of the bioturbator,*Hydrobia ulvae*." *J. Mar Res*, 61, 823-851.

Orvain, F.,Sauriau, P.-G., Le Hir, P., Guillou, G., Cann, P., Paillard, M. (2007) "Spatio-temporal variations in intertidal mudflat erodability: Marennes-Oléron Bay, western France." *Cont. Shelf Res.*, 27, 1153-1173.

Parchure, T.M., Mehta, A.J. (1985) "Erosion of soft cohesive sediment deposits." *J. Hydraul. Eng.*, 111(10), 1308-1326.

Paterson, D.M. (1989) "Short term changes in the erodibility of intertidal cohesive sediments related to the migratory behaviour of epipelic diatoms." *Limnol. Oceanogr.* 34, 223-234.

Ravens, T.M. (2007) "Comparison of Two Techniques to Measure Sediment Erodibility in the Fox River, Wisconsin." *J Hydraul. Eng*, 133(1) , 111-115.

Schlichting, H. (1979) *Boundary Layer Theory.* McGraw-Hill, New York, NY, pp 817.

Shields, A. (1936) "Anwendung der Aehnlichkeitsmechanik und Turbulenzforhcung auf die Geschiebebewegung." Mitt PreussVersuchsanstalt fur Wasserbau und Schiffbau, 26, Berlin.

Soulsby, R. (1997) *Dynamics of Marine Sands.* Thomas Telford Ltd., London, pp 249.

Sugihara, G., May, M. (1990) "Applications of fractals in ecology." *Trends Ecol. Evol.*, 5, 79-86.

Tolhurst, T.J., Black, K.S., Shayler, S.A., Mather, S., Black, I., Baker, K., Paterson, D.M. (1999) "Measuring the *in situ* erosion shear stress of intertidal sediments with the Cohesive Strength Meter (CSM)." *Est. Coast. Shelf Sci.*, 49, 281-294.

Tolhurst, T.J., Reithmüller, R., Paterson, D.M. (2000) "*In situ* versus laboratory analysis of sediment stability from intertidal mudflats." *Cont. Shelf Res.*, 20, 1317-1334.

Tolhurst, T.J., Black, K.S., Paterson, D.M., Mitchener, H., Termaat, R., Shayler, S.A. (2000) "A comparison and measurement standardisation of four *in situ* devices for measuring the erosion shear stress of intertidal sediments." *Cont. Shelf Res.*, 20(2) , 1397-1418.

Tolhurst, T.J., Black, K.S., Paterson, D.M. (2009) "Muddy sediment erosion: insights from field studies." *J Hydraul. Eng*, 135(2) , 73-87.

Verdelhos, T., Neto, J.M., Marques, J.C., Pardal, M.A. (2005) "The effect of eutrophication abatement on the bivalve *Scrobicularia plana*." *Est. Coast. Shelf Sci.*, 63 , 261-268.

Widdows, J., Brinsley, M.D., Bowley, N., Barret, C. (1998) "A benthic annular flume for *in situ* measurement of suspension feeding/biodeposition rates and erosion potential of intertidal cohesive sediments." *Est. Coast. Shelf Sci.*, 46, 27-38.

Widdows, J., Brown, S., Brinsley, M.D., Salkield, P.N., Elliot, M. (2000) "Temporal changes in intertidal sediment erodability: influence of biology and climatic factors." *Cont. Shelf Res.*, 20(10-11), 1275-1290.

Widdows, J., Friend, P.L., Bale, A.J., Brinsley, M.D., Pope, N.D., Thompson, C.E.L. (2007) "Inter-comparison between five devices for determining erodability of intertidal sediments." *Cont. Shelf Res.*, 27(8), 1174-1189.

Wright, L.D., Friedrichs, C.T., Hepworth, D.A. (1997) "Effects of benthic biology on bottom boundary layer processes." Dry Tortugas Bank, Florida Keys. *Geo-Mar. Lett.*, 17(4), 291-298.

List of Figures

Material	Diameter range (mm)	Density (kg m^{-3})	Relative roughness D_{50}/D_h	Re_c	f
Sand	0.19-0.21	2700	0.0063	2.5	NC
Sand	1.25-1.6	2700	0.0445	41	0.13±0.03
Steel	1.25-1.6	7650	0.0445	89	0.14±0.03
Lead	1.6-2.0	10965	0.0563	164	0.18±0.03
Lead	2.0-2.5	10965	0.0703	237	0.22±0.02

Table 1: *Caracteristics of the five categories of calibrated particles used in Shields experiments (Fig. 4) and the bed friction factors derived from bed shear stress vs pump discharge curves.*

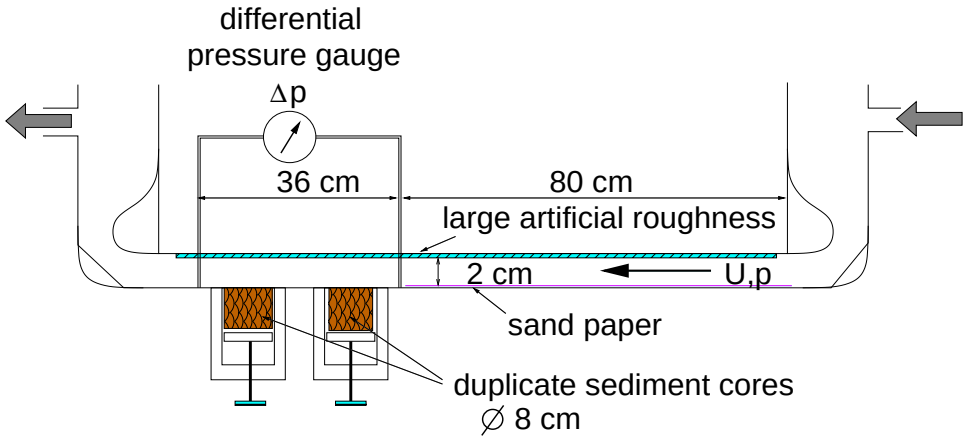

Figure 1: *Schematic of Erodimetre erosion tunnel, designed by the Institut Français de Recherche pour l'Exploitation de la MER (Le Hir et al. 2006).*

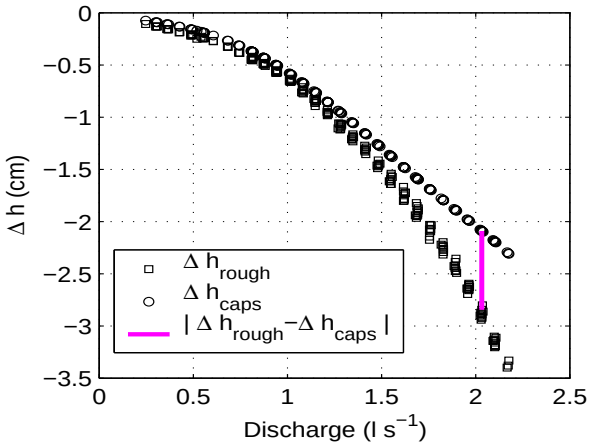

Figure 2: *Head loss for increasing flow discharge with plexiglass caps (circle) and with mud cores (square): excess of bed shear stress due to mud roughness for a given discharge is proportional to the distance between the two curves as displayed by the thick vertical line.*

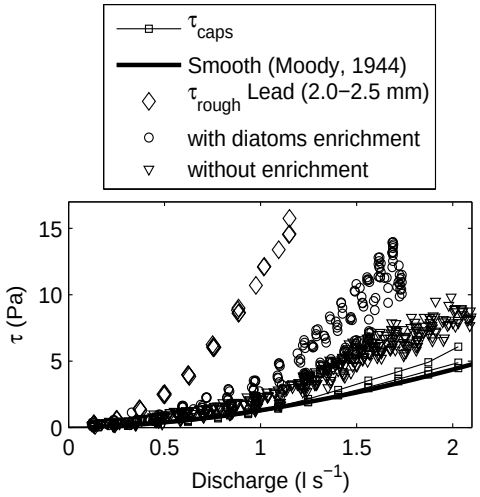

Figure 3: *Bed shear stress (τ) versus pump discharge in the mesocosm experiments. Bed shear stress measured in three different experiments with plexiglass caps (open squares), in the experiment with a plane bed formed by 2.25 mm calibrated particles (open diamonds), and the smooth bed reference (thick line, using Moody (1944) smooth friction factor in equation 2) are displayed.*

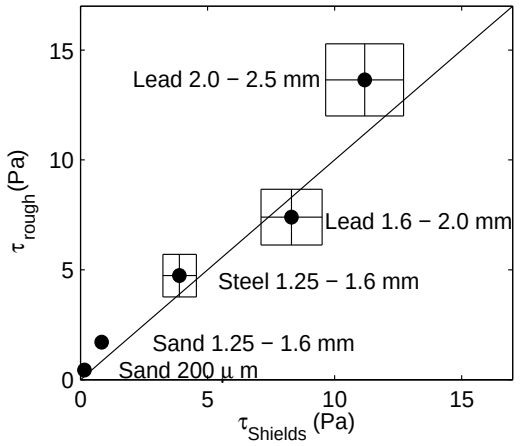

Figure 4: *Bed shear stress derived from head loss measurements (τ_{rough}) (filled circle) versus bed shear stress for incipient motion according to Shields criteria $\tau_{Shields}$ (equation 4) of five calibrated particles. Error bars on τ_{rough} correspond to uncertainty on incipient motion determination while error bars on $\tau_{Shields}$ correspond to the bed shear stress derived from Shields criteria for the lower and upper diameters for each calibrated particles' set.*